

Low Voltage Ride Through Enhancement Based on Improved Direct Power Control of DFIG under Unbalanced and Harmonically Distorted Grid Voltage

A. R. Nafar Sefiddashti¹, G. R. Arab Markadeh^{2*}, A. Elahi¹, R. Pouraghababa³

¹Department of Electrical Engineering, Shahrekord University, Shahrekord, Iran

²Member of Center of Excellence for Mathematics, Department of Electrical Engineering, Shahrekord University, Shahrekord, Iran

³Esfahan Regional Electrical Company

ABSTRACT

In the conventional structure of the wind turbines along with the doubly-fed induction generator (DFIG), the stator is directly connected to the power grid. Therefore, voltage changes in the grid result in severe transient conditions in the stator and rotor. In cases where the changes are severe, the generator will be disconnected from the grid and consequently the grid stability will be attenuated. In this paper, a completely review of conventional methods for DFIG control under fault conditions is done and then a series grid side converter (SGSC) with sliding mode control method is proposed to enhance the fault ride through capability and direct power control of machine. By applying this controlling strategy, the over current in the rotor and stator windings will totally be attenuated without using additional equipments like as crowbar resistance; Moreover, the DC link voltage oscillations will be attenuated to a great extent and the generator will continue operating without being disconnected from the grid. In addition, the proposed method is able to improve the direct power control of DFIG in harmonically grid voltage condition. To validate the performance of this method, the simulation results are presented under the symmetrical and asymmetrical faults and harmonically grid voltage conditions and compared with the other conventional methods.

KEYWORDS: Doubly-fed induction generator, Fault ride through capability, Sliding mode control, Series compensator.

1. INTRODUCTION

In recent years, wind energy has made the most progress among other energy resources. The more development of wind energy utilization in electric power systems, the poorer performance of the wind farms in the case of fault. The reason is that the disconnection of the wind turbine from the grid causes instability. When a voltage drop occurs in the grid, it affects the connection point of the grid and generator and causes a sudden voltage drop in the stator which consequently increases the rotor current and the DC link voltage of back to back converter [1].

In such circumstances, the generator may be disconnected from the grid. This may, furthermore, leads to the frequency and voltage control problems. Therefore, it is recommended that the wind turbines stay connected and actively help in the stability of the power system during the fault occurrence. In other words, wind turbine should have the fault ride through capability.

With the increasing penetration of wind plants in the power systems to ensure the quality of the grid, several grid regulations have been established. These regulations define the performance limit of wind turbines connected to the grid in terms of power factor, frequency range, voltage variations and the fault ride through capability. To meet the grid regulations, the wind turbines should be capable of neutralizing the additional currents which are the

Received: 28 May 2015

Revised: 10 Dec. 2015

Accepted: 25 Dec. 2015

*Corresponding author:

G. R. Arab Markadeh (arab-gh@eng.sku.ac.ir)

© 2016 University of Mohaghegh Ardebil

result of the transient voltage drop and continue power transmission to the grid during the short circuit. Fig. 1 presents the grid regulations, according to the voltage changes for different countries [2].

There are many ways to protect and prevent damage to the wind turbine. In order to prevent excessive current damage to the rotor side converter, the generator rotor circuit will be blocked with a series short circuit resistor and the rotor side converter (RSC) which is called the crowbar [3-6]. Since the rotor side converter is disconnected at the time of the fault, it makes impossible to control the reactive power.

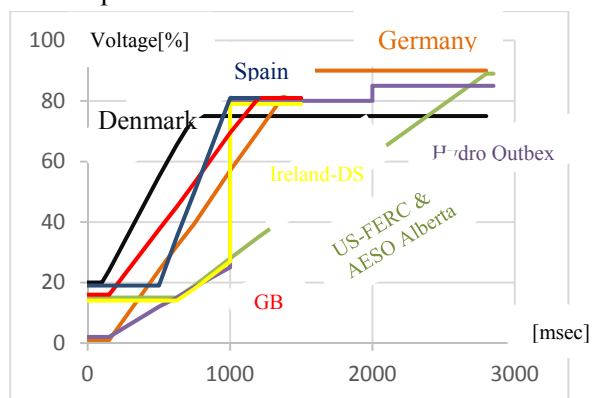


Fig. 1. The voltage through drop requirement and the grid regulations for different countries [2]

Each of the above mentioned references applied different controlling method to control the RSC and the grid side converter (GSC). The oscillations in the rotor and stator current are the result of the DC component of the stator flux in the case of a fault [7]. Therefore, the demagnetization method is applied to control RSC in Ref. [7]. So if the DC component of the rotor current reduces, the stator linkage can be demagnetized and then the oscillation of the current will be attenuated. As well as, a crowbar along with a hysteresis controller is used for controlling. Since there was no reactive power control at the time instant of RSC disconnection, the transient time to get to the desired performance will be reduced by the reduction of the crowbar connection duration time. While in other references, the crowbar is still active at the total fault time or even some time after that.

In Ref. [8] the application of a series resistor in the stator or rotor circuit is proposed to limit the machine currents at fault time. The vector control is

used in this reference to control the converters; however, the DC link voltage is not controlled.

Utilizing a series compensator with the stator windings another strategy which helps to enhance the performance compared with the other methods [9-13]. In this method, the stator voltages of the disturbed lines will be refined by this compensator and the generator continues operating without getting disconnected from the grid. In Ref. [9], the RSC and GSC are controlled based on vector control method with the aim of controlling the active and reactive powers and limiting the currents in the case of an asymmetric fault. As well as, a proportional+resonant controller is used for the series converter. This structure has to tolerate the total power through of the grid because of the existence of a series converter in the grid. Furthermore, this controlling method is not robust to the parameters' changes because of the application of PI controllers; therefore, it cannot maintain the system stability in the case of fault occurrence.

In Ref. [10], the vector control method is applied for both converters to control the active and reactive power and the DC link voltage. As well as, the series converter is used to inject the desired voltage to the grid voltage in order to balance the stator voltages.

In Ref. [11], the control structure of the back to back converters is the same as [10], but an adaptive fuzzy PI controller is used for series converter. In Ref. [12], using a supercapacitor energy storage system is used to store the rotor energy in fault conditions and return it to the network whenever needed.

In most of the above mentioned references, the DC link voltage regulation and the rotor current limitation were not both concurrently controlled in the case of the symmetric and asymmetric faults.

In Ref. [13], a nine-switches inverter with two independent output voltage is proposed to be used instead of GSC and series converter. It is known that multi-output inverters increase the voltage stress of DC link capacitor and the switching losses because of the higher switching frequency in comparison with the conventional inverters.

Another method for the rotor current limitation in fault conditions is proposed in Ref. [14], in which the additional energy of the wind turbine is stored in

the rotor moment of inertia by increasing the rotor speed with the pitch angle control; however, it is impossible due to the mechanical system's time constant.

A sensitivity analysis approach integrated with a novel hybrid approach combining wavelet transform, particle swarm optimization and an adaptive-network-based fuzzy inference system known as Wavelet-ANFIS-PSO is proposed in Ref. [15] to acquire the optimal control of DFIG based wind generation. In Ref. [16], a multi-objective economic load dispatch model is developed for the system consisting of both thermal generators and wind turbines. Using two optimization methods, sequential quadratic programming and particle swarm optimization, the system are optimally scheduled. The objective functions are total emission and a total profit of units.

In Ref. [17] the sliding mode control method without decomposition of negative and positive sequences of unbalanced variables is used for control of active and reactive power under unbalanced and harmonic distorted grid voltage, but stator voltages and currents and rotor currents are still unbalanced and DC link voltage is not controlled properly.

In Ref. [18] a DC-capacitor current control method is investigated for a grid-side converter to eliminate the negative impact of unbalanced grid voltage on the DC-capacitor. Although Vdc fluctuations is reduced, the oscillation and unbalance of other variables still exist.

In this paper, a series compensator, placed in the DFIG stator, will be used to control the rotor and stator currents in the case of symmetric and asymmetric fault. Using this compensator, there is no need for a crowbar. Moreover, for the robustness of the controller structure respect to the changes in the machine parameters, the sliding controller will be used to control the series compensator converter and RSC and GSC converters. This compensator is directly fed by the DC link between the two RSC and GSC converters and at the same time, it has the fault ride through capability in the case of symmetric and asymmetric faults. Due to the rapid response rate of the controller, there would not be any oscillations in the rotor and stator currents in the case

of different types of fault. Furthermore, the DC link voltage regulation and control of active and reactive power and torque is well achieved.

The present paper has the following structure. In Section II, Introducing different DFIG structures with additional equipment in fault ride through. In Section III, the generator has been modeled. In Section IV, all three converters have been investigated using sliding mode control. In Section V, simulation results using this method of control are compared with vector control method presented in Ref. [9] and finally, the general conclusion of this paper is presented in the last Section.

2. FAULT RIDE THROUGH CONTROL STRUCTURES

As it was stated in the previous parts, different topologies exist for the fault ride through control. In one of these structures, while a fault happens in the grid, the rotor side converter will be disconnected and the rotor windings will have a short circuit with a series of external resistors known as a crowbar. An example of this structure is shown in Fig. 2 [4]. In many papers, the three-phase crowbar structure with different controlling methods is simultaneously used by RSC and GSC for the fault ride through [5, 6].

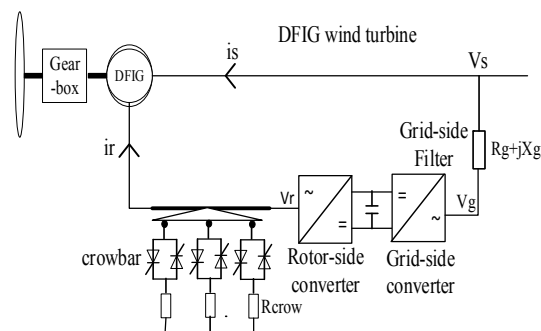


Fig. 2. Crowbar three-phase structure and its placement [4]

To reduce the rating power of crowbar switches, the various structures of crowbar connections are presented in Ref. [19]. In this reference, the allowable voltage of each switch and the current of each switch in the Delta connection will be reduced to 0.577 by the use of Wye connection (Fig. 3).

Another topology proposed in Ref. [20] for the fault ride through is a switching resistive load which is paralleled with the DC link capacitor. This structure prevent the DC link voltage to reach to an unauthorized value in the fault condition (Fig. 4).

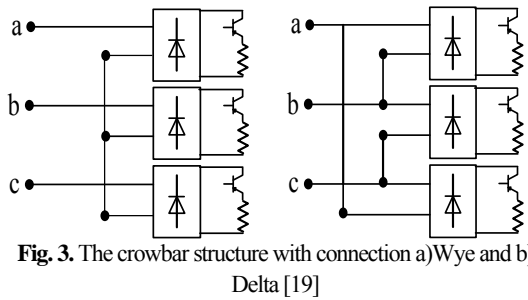


Fig. 3. The crowbar structure with connection a) Wye and b) Delta [19]

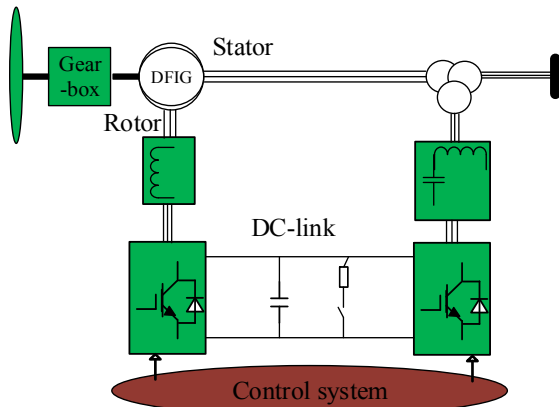


Fig. 4. The placement of DC brake chopper [20]

Another structure, proposed in Ref. [21], is the simultaneous use of DC brake chopper and crowbar. As shown in Fig. 5, this strategy will be capable of limiting the rotor current and the DC link voltage to an authorized limit.

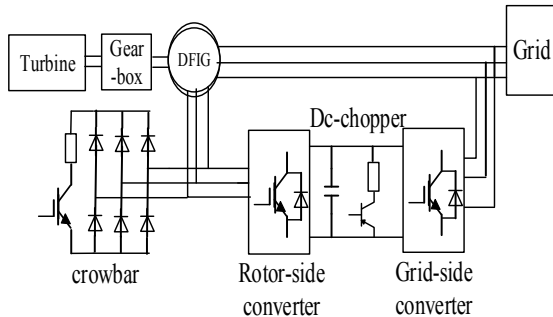


Fig. 5. Simultaneous use of DC brake chopper and crowbar [21]

In Ref. [8], limiting the stator and rotor currents in the fault condition has been achieved through the application of a controllable resistor in the stator circuit. As presented in Fig. 6, when the bidirectional switch is turned off, the resistor enters the circuit and is able to limit the rotor and stator currents.

One of the other methods for the fault ride through control is using a series compensator to inject a voltage in the stator circuit in fault condition [9], [22]. This structure in some research works known as dynamic voltage restore (DVR) and is depicted in Fig. 7. In [9], the DC link capacitor of

DVR is an independent capacitor while in Ref. [22], a common capacitor is used for RSC, GSC and DVR.

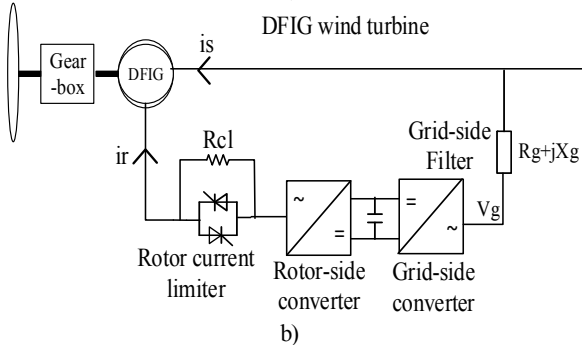
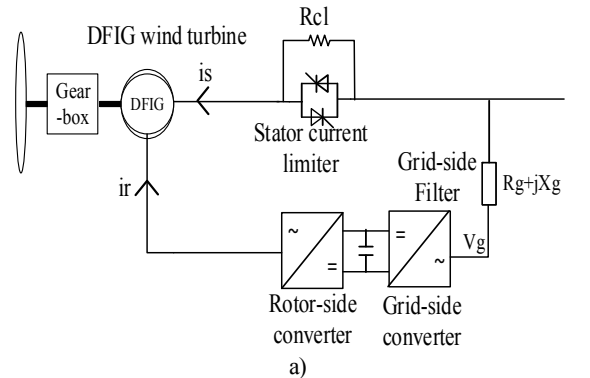


Fig. 6. Using the series crowbar structure in a) stator, b) rotor [8]

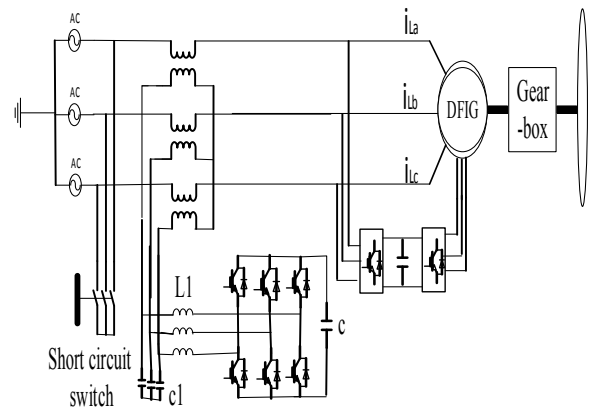


Fig. 7. Using a series compensator and feeding it with a separate capacitor [9]

Besides the structures which are based on the series compensator, another structure has been proposed in Ref. [12] in which not only the series compensator is fed by the DC link capacitor, but also another storage capacitor or battery, parallel with the DC link capacitor is also considered to store the additional energy absorbed from the RSC in the fault condition. In the other words, any electrical generated energy in fault condition will be stored in this supercapacitor and after fault clearing,

the energy will be transferred to the grid. Fig. 8 presents the structure of this compensator.

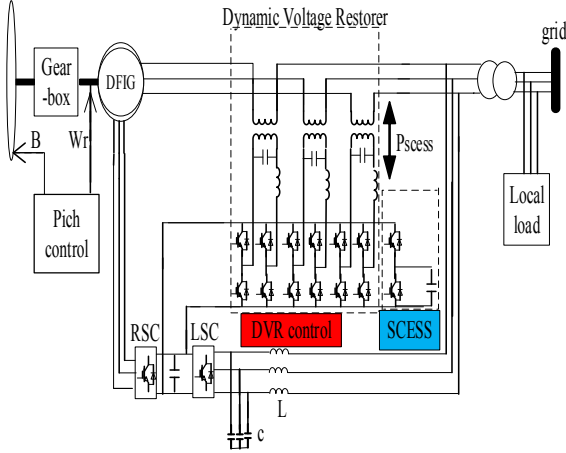


Fig. 8. The series compensator along with the energy storage capacitor (battery) [12, 24]

3. MATHEMATICAL MODEL

The equivalent circuit of a DFIG in the stationary reference frame is presented in Fig. 9. In this circuit, all the rotor parameters are transferred to the stator side. The rotor and stator voltage equations are as follows.

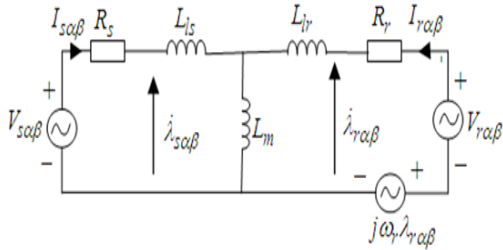


Fig. 9. The equivalent circuit of the induction machine in the stationary reference frame

$$\vec{v}_{s\alpha\beta} = R_s \vec{i}_{s\alpha\beta} + \frac{d\vec{\psi}_{s\alpha\beta}}{dt} \quad (1)$$

$$\vec{v}_{r\alpha\beta} = R_r \vec{i}_{r\alpha\beta} + \frac{d\vec{\psi}_{r\alpha\beta}}{dt} + j\omega_r \vec{\psi}_{r\alpha\beta} \quad (2)$$

where R_s and R_r are stator and rotor resistances.

The flux linkage of the stator and rotor will be obtained from the Eqs. (3) and (4).

$$\vec{\psi}_{s\alpha\beta} = L_s \vec{i}_{s\alpha\beta} + L_m \vec{i}_{r\alpha\beta} \quad (3)$$

$$\vec{\psi}_{r\alpha\beta} = L_r \vec{i}_{r\alpha\beta} + L_m \vec{i}_{s\alpha\beta} \quad (4)$$

where L_s , L_r and L_m are the stator, rotor and the magnetizing inductances respectively.

By instituting the Eqs. (3) and (4) in Eqs. (1) and (2) and the calculation of the space phasor of the stator currents, we have:

$$\frac{d\vec{i}_{s\alpha\beta}}{dt} = \frac{1}{L_r} [L_r \vec{V}_{s\alpha\beta} - L_m \vec{V}_{r\alpha\beta} - R_s L_r \vec{i}_{s\alpha\beta} \quad (5)$$

$$-j\omega_r L_m (L_r \vec{i}_{r\alpha\beta} + L_m \vec{i}_{s\alpha\beta}) + L_m R_r \vec{i}_{r\alpha\beta}]$$

In the above equation, $L_r' = L_s L_r - L_m^2$.

Equation (6) presents the relation between active and reactive power of the stator with machine variables.

$$\begin{cases} P_s = \frac{3}{2} (v_{\alpha s} i_{\alpha s} + v_{\beta s} i_{\beta s}) \\ Q_s = \frac{3}{2} (v_{\beta s} i_{\alpha s} - v_{\alpha s} i_{\beta s}) \end{cases} \quad (6)$$

4. CONTROL STRUCTURE

4.1. DFIG vector control

As it was mentioned in section one, one of the ways for the fault ride through is the application of the series compensator on the grid. In Ref. [9], a vector control method has been used to control the active and reactive powers of the stator. Furthermore, to control the DC link voltage and the GSC reactive power, the vector control method is used. The series converter control has been achieved using a proportional+ resonant controller. To control the series converter, first the voltage phase of the grid will be identified through a phase lock loop by which the positive and negative sequences of the grid voltage will be obtained. Now, the series converter sets the amount of the injected voltage to each phase through the obtained values. By this method, a safe and normal voltage is achievable. Since the PI controller is used for controlling in this reference, this controller is not tolerant of the parameter's changes. The controlling block diagram used is shown in Appendix C.

4.2. SMC of the RSC

RSC is generally used to control the active and reactive power of the stator and the rotor speed. In this paper, the active and reactive powers are controlled by RSC.

Considering the controlling variables of P_s and Q_s for RSC, the sliding surface will be considered with integral type.

$$\begin{aligned} S_{P_s} &= e_{P_s} + k_{P_s} \int e_{P_s} dt, e_{P_s} = P_s^* - P_s \\ S_{Q_s} &= e_{Q_s} + k_{Q_s} \int e_{Q_s} dt, e_{Q_s} = Q_s^* - Q_s \end{aligned} \quad (7)$$

k_{P_s} and k_{Q_s} are positive constants. Moreover, e_{P_s} and e_{Q_s} are the errors of active and reactive powers of the stator. By the derivation of the sliding surface with respect to time in Eq. (7), we have:

$$\begin{aligned}\dot{S}_{P_s} &= \dot{P}_s^* - \dot{P}_s + k_{P_s}(P_s^* - P_s) \\ \dot{S}_{Q_s} &= \dot{Q}_s^* - \dot{Q}_s + k_{Q_s}(Q_s^* - Q_s)\end{aligned}\quad (8)$$

\dot{P}_s and \dot{Q}_s can be obtained based on Eq. (6) as follows:

$$\begin{cases} \frac{dP_s}{dt} = \frac{3}{2} \left(i_{\alpha s} \frac{dv_{\alpha s}}{dt} + i_{\beta s} \frac{dv_{\beta s}}{dt} + v_{\alpha s} \frac{di_{\alpha s}}{dt} + v_{\beta s} \frac{di_{\beta s}}{dt} \right) \\ \frac{dQ_s}{dt} = \frac{3}{2} \left(i_{\alpha s} \frac{dv_{\beta s}}{dt} + v_{\beta s} \frac{di_{\alpha s}}{dt} - i_{\beta s} \frac{dv_{\alpha s}}{dt} - v_{\alpha s} \frac{di_{\beta s}}{dt} \right) \end{cases}\quad (9)$$

In the case of a balanced voltage source, we have:

$$\begin{cases} V_{\alpha s} = V_m \cos(\omega_s t) \\ V_{\beta s} = V_m \sin(\omega_s t) \end{cases}\quad (10)$$

Therefore, the voltage deviation respect to time obtained as follows:

$$\begin{cases} \frac{d}{dt} V_{\alpha s} = -\omega_s V_m \sin(\omega_s t) = -\omega_s V_{\beta s} \\ \frac{d}{dt} V_{\beta s} = \omega_s V_m \cos(\omega_s t) = \omega_s V_{\alpha s} \end{cases}\quad (11)$$

By separating Eq. (5) to real and imaginary parts and substituting Eq. (11) in Eq. (9) can be rewritten as:

$$\begin{aligned} \frac{d}{dt} \begin{pmatrix} P_s \\ Q_s \end{pmatrix} &= \frac{3L_m}{2L_r} \begin{pmatrix} -V_{\alpha s} & -V_{\beta s} \\ -V_{\beta s} & V_{\alpha s} \end{pmatrix} \begin{pmatrix} V_{\alpha r} \\ V_{\beta r} \end{pmatrix} \\ &+ \begin{pmatrix} R_r V_{\alpha s} - \omega_r L_r V_{\beta s} & R_r V_{\beta s} + \omega_r L_r V_{\alpha s} \\ R_r V_{\beta s} + \omega_r L_r V_{\alpha s} & -R_r V_{\alpha s} + \omega_r L_r V_{\beta s} \end{pmatrix} \begin{pmatrix} i_{\alpha r} \\ i_{\beta r} \end{pmatrix} \\ &+ \begin{pmatrix} \frac{L_r L_r}{L_m} (V_{\alpha s}^2 + V_{\beta s}^2) \\ 0 \end{pmatrix} + \begin{pmatrix} \frac{R_s L_r}{L_r} & -(\omega_r L_m^2 + \omega_s) \\ -(\omega_r L_m^2 + \omega_s) & \frac{R_s L_r}{L_r} \end{pmatrix} \begin{pmatrix} P_s \\ Q_s \end{pmatrix} \end{aligned}\quad (12)$$

By substituting Eq. (12) in Eq. (8) the \dot{S} yields:

$$\frac{d}{dt} \begin{pmatrix} S_{P_s} \\ S_{Q_s} \end{pmatrix} = -D \frac{d}{dt} \begin{pmatrix} P_s \\ Q_s \end{pmatrix} + \begin{pmatrix} k_{P_s} (P_s^* - P_s) \\ k_{Q_s} (Q_s^* - Q_s) \end{pmatrix} = F + DV_{r\alpha\beta}\quad (13)$$

Finally the control input can be expressed as:

$$\begin{pmatrix} V_{\alpha r} \\ V_{\beta r} \end{pmatrix} = -D^{-1} \left(F + \begin{pmatrix} k_{P_s} \text{sign}(S_{P_s}) \\ k_{Q_s} \text{sign}(S_{Q_s}) \end{pmatrix} \right)\quad (14)$$

4.3. SMC of the GSC

The controlling objectives of the grid side converter control are: 1) DC link voltage control and 2) the grid side reactive power control. To design the GSC controller, first a sliding surface, as Eq. (15), should be considered to attain the controlling objectives.

$$\begin{aligned} S_{V_{dc}} &= \dot{e}_{V_{dc}} + \lambda_1 e_{V_{dc}} + \lambda_2 \int e_{V_{dc}} dt, \\ e_{V_{dc}} &= V_{dc}^* - V_{dc} \\ S_{Q_g} &= e_{Q_g} + \lambda_{Q_g} \int e_{Q_g} dt, \\ e_{Q_g} &= Q_g^* - Q_g \end{aligned}\quad (15)$$

By the derivation of the sliding surface, we will have:

$$\begin{aligned} \dot{S}_{V_{dc}} &= -\ddot{V}_{dc} - \lambda_1 \dot{V}_{dc} + \lambda_2 (V_{dc}^* - V_{dc}) \\ \dot{S}_{Q_g} &= \dot{Q}_g^* - \dot{Q}_g + \lambda_{Q_g} (Q_g^* - Q_g) \end{aligned}\quad (16)$$

λ_1, λ_2 and λ_{Q_g} are positive constants. The electrical equations of this converter in the stationary reference frame are as follows:

$$CV_{dc} \frac{dV_{dc}}{dt} = P_g - P_r\quad (17)$$

In the above equation,

$$P_g = \frac{3}{2} (e_{n\alpha} i_{g\alpha} + e_{n\beta} i_{g\beta})\quad (18)$$

$$Q_g = \frac{3}{2} (e_{n\beta} i_{g\alpha} - e_{n\alpha} i_{g\beta})\quad (19)$$

$$\vec{e}_n = \vec{U}_{gn} + R_g \vec{i}_g + L_g \frac{d\vec{i}_g}{dt}\quad (20)$$

P_g and Q_g are the active and reactive power of the grid, respectively and \vec{e}_n is the voltage space phasor of the grid. The relation between the voltages of each inverter base and the two-axial frame of $\alpha\beta$ is as follows:

$$\begin{aligned} \begin{bmatrix} v_{g\alpha} \\ v_{g\beta} \end{bmatrix} &= M_2 M_1 U_g \\ M_1 &= \frac{1}{3} \begin{bmatrix} 2 & -1 & -1 \\ -1 & 2 & -1 \\ -1 & -1 & 2 \end{bmatrix}, M_2 = \frac{2}{3} \begin{bmatrix} 1 & -1 & -1 \\ 0 & \sqrt{3} & -\sqrt{3} \\ 0 & 2 & 2 \end{bmatrix} \end{aligned}\quad (21)$$

In the above relation, M_1 is the transformation matrix between U_r and the rotor winding voltage, M_2 is the Clark transformation matrix.

By the derivation of Eqs. (18) and (19) and separating the real and imaginary sequences of the space phasor derivation of the grid current from the relation Eq. (20) and instituting in Eq. (16), we have:

$$\begin{aligned} \dot{S}_{V_{dc}} &= F_{V_{dc}} \\ \dot{S}_{Q_g} &= F_{Q_g} - \frac{3}{2L_g} \begin{bmatrix} -e_{n\alpha} & -e_{n\beta} \\ CV_{dc} & CV_{dc} \\ -e_{n\beta} & e_{n\alpha} \end{bmatrix} \begin{bmatrix} v_{g\alpha} \\ v_{g\beta} \end{bmatrix} \end{aligned}\quad (22)$$

In relation Eq. (22), $F_{V_{dc}} Q_g$ is a function of state variables, the entrance reference values and their derivations; however, it is not related the controlling entrances of $v_{g\alpha}$ and $v_{g\beta}$. By instituting Eq. (21) in Eq. (22), we have:

$$\dot{S}_{V_{dc} Q_g} = F_{V_{dc} Q_g} - \frac{C_{V_{dc} Q_g}}{K \frac{M_2 M_1}{M}} U_g \quad (23)$$

Since $\dot{S}_{V_{dc} Q_g}$ varies with time, a new sliding surface is used to obtain the control rule which is related to the previous sliding surface ($S_{V_{dc} Q_g}$) as follows [25, 26]:

$$S_{V_{dc} Q_g}^* = C_{V_{dc} Q_g}^+ S_{V_{dc} Q_g} \quad (24)$$

In this relation, $C_{V_{dc} Q_g}^+$ is the Moor-Penrose pseudo-inverse matrix for $C_{V_{dc} Q_g}$. Similar to the rotor side controller, the control rule for the grid side parallel converter is:

$$U_g = u_0 \operatorname{sgn}(S_{V_{dc} Q_g}^*) \quad (25)$$

4.4. SMC of the SGSC

The main objective in the series converter control is the injection of the balanced or imbalanced voltage (or both) to the grid so that the stator voltages and as a consequence, stator and rotor currents get balanced. A balanced voltage in the stator reduces the oscillations of the electromagnetic torque and other under control variables. Therefore, the following sliding surfaces can be defined:

$$\begin{cases} s_{v_\alpha} = \lambda_{v_\alpha} \int e_{v_\alpha} dt, e_{v_\alpha} = v_{inj_\alpha}^* - v_{inj_\alpha} \\ s_{v_\beta} = \lambda_{v_\beta} \int e_{v_\beta} dt, e_{v_\beta} = v_{inj_\beta}^* - v_{inj_\beta} \end{cases} \quad (26)$$

λ_{v_α} and λ_{v_β} are the positive constants. Assuming that $R_{gs} = 0$, the relation between the injected voltage in line and the voltage of each inverter leg in the stationary reference frame will be obtained from Eq. (27).

$$\begin{aligned} V_{inj_\alpha} &= v_{conv_\alpha} \\ V_{inj_\beta} &= v_{conv_\beta} \end{aligned} \quad (27)$$

The reference voltages for the series converter will be obtained from the following relations:

$$\begin{cases} v_{inj_\alpha}^* = e_{n\alpha} - v_{s_\alpha}^* \\ v_{inj_\beta}^* = e_{n\beta} - v_{s_\beta}^* \end{cases} \quad (28)$$

In the above relation, $v_{s_\alpha}^*$ and $v_{s_\beta}^*$ are the stator reference voltages, $v_{inj_\alpha}^*$ and $v_{inj_\beta}^*$ are the reference voltages of the grid side series converter in the stationary reference frame and $e_{n\alpha}$ and $e_{n\beta}$ are the desired voltages for the grid. By the derivation of the relation Eq. (26) and replacing from Eq. (27) in terms of v_{conv_α} and v_{conv_β} , we will have:

$$\begin{bmatrix} \dot{s}_{v_\alpha} \\ \dot{s}_{v_\beta} \end{bmatrix} = \begin{bmatrix} \lambda_{v_\alpha} v_{inj_\alpha}^* \\ \lambda_{v_\beta} v_{inj_\beta}^* \end{bmatrix} - \begin{bmatrix} \lambda_{v_\alpha} & 0 \\ 0 & \lambda_{v_\beta} \end{bmatrix} \begin{bmatrix} v_{conv_\alpha} \\ v_{conv_\beta} \end{bmatrix} = A + T \begin{bmatrix} v_{conv_\alpha} \\ v_{conv_\beta} \end{bmatrix} \quad (29)$$

Therefore, the control rule for the switching of the series converter can be obtained as follows:

$$\begin{bmatrix} v_{conv_\alpha} \\ v_{conv_\beta} \end{bmatrix} = \frac{-1}{T} \left[A + \begin{bmatrix} \lambda_{v_\alpha} \operatorname{sign}(s_{v_\alpha}) \\ \lambda_{v_\beta} \operatorname{sign}(s_{v_\beta}) \end{bmatrix} \right] \quad (30)$$

5. SIMULATION RESULTS

In this section, the simulation results for a 2 MW DFIG are presented (Appendix A). The controllers' coefficients are presented in Appendix B Simulation is performed in five tests.

Test 1: Three-phase symmetric fault which reduces the PCC voltage to 95% of the nominal grid voltage with the proposed method.

Test 2: Two-phase asymmetric fault which reduces the voltage to 63% of the nominal grid voltage at the PCC point with method used in Ref. [9].

Test 3: Two-phase asymmetric fault which reduces the voltage to 95% of the nominal grid voltage at the PCC point with the proposed method.

Test 4: DFIG with SGSC is connected to a network with voltage harmonic amplitudes: V5=6% and V7=5%.

Test 5: The robustness of the proposed control algorithm against parameter variations is checked.

In Fig. 10, the overall scheme of the system investigated in this paper is presented. In Appendix, the system parameters are provided. Since most faults in the control systems are of the asymmetric type, the simulation results of both symmetric and asymmetric faults are presented here.

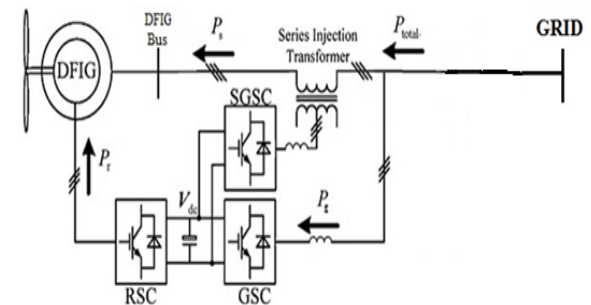


Fig. 10. the overall scheme of the proposed system

Test 1

In Fig. 11, the simulation results for the three-phase symmetric fault which reduces the voltage to 95% of the nominal grid voltage at the PCC point is

presented. As it is shown in the wave shape of the PCC voltage (Fig. 11.a), the fault happens at 1.7 s which takes 150 ms time. The stator and rotor currents continue without any fluctuation at the fault time (Fig. 11.b). The DC link voltage reaches to the desired value of 1200V after a small oscillation. It is worth mentioning that while the above mentioned points are desirable in the control strategy, the active and reactive powers and the electromagnetic torque will be successfully controlled as well (Fig. 11. e, f and g, respectively). As the results indicate, the proposed strategy limits the current amplitude at a desired value even at fault condition and the DC link voltage is regulated. At the same time, the torque and power control is well achieved.

Test 2

The simulation results with the structure proposed in Ref. [9] are presented in Fig. 12. As it can be seen a two-phase fault with the grid voltage nominal value of 63% at the 1.7 s causes the voltage drop and the fault continues for 150 ms. Stator and rotor voltages have oscillations even after fault clearing to reach to the desired values (Fig 12. b and c). In this control method, the active and reactive power control has been achieved; however, as it is shown in Fig. 12. d, they have oscillations at the fault time. As well as, the DC link voltage control has not been done in this reference.

Test 3

Figure 13 is the simulation results in the two-phase fault condition which the voltage drop in two phases is 95% of the nominal voltage at the PCC point. The results for this type of faults have been attained without any change in the controller and system structure. As it is shown in Fig. 13. a, the fault is occurred at 1.7 s and takes 150 ms time. The stator and rotor currents will continue without any oscillation at the fault time (Fig. 13. b and c). The DC link voltage, with a small oscillation at the start of the fault time instant, tends to its reference value of 1200 V. Similar to the symmetric fault, the control of active and reactive powers and the electromagnetic torque is possible (Fig. 13 e, f and g).

Test 4

In this test, DFIG simulation is presented with harmonic distorted grid voltage. It is assumed that the network voltage, in addition to fundamental

harmonic, has fifth and seventh order of harmonics with 8% THD. The simulation results are shown in Fig. 14. Since the resultant rotating magnetic field of the fifth order harmonic is in the opposite direction of rotating field caused by fundamental harmonic, the existence of this harmonic order creates braking torque on machine shaft which will reduce shaft lifetime and increase T_e ripple.

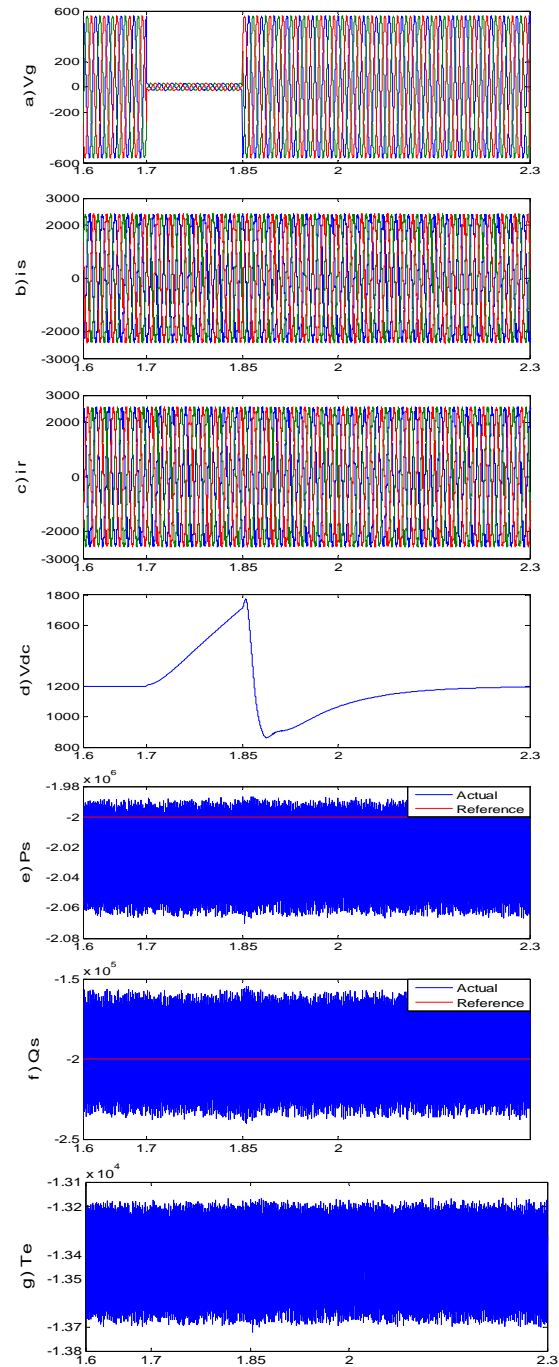


Fig. 11. Simulation results for the three-phase fault with 95% decreasing of nominal grid voltage a) grid voltage, b) stator current, c) rotor current, d) DC link voltage, e) stator's active power, f) stator's reactive power and g) electromagnetic torque.

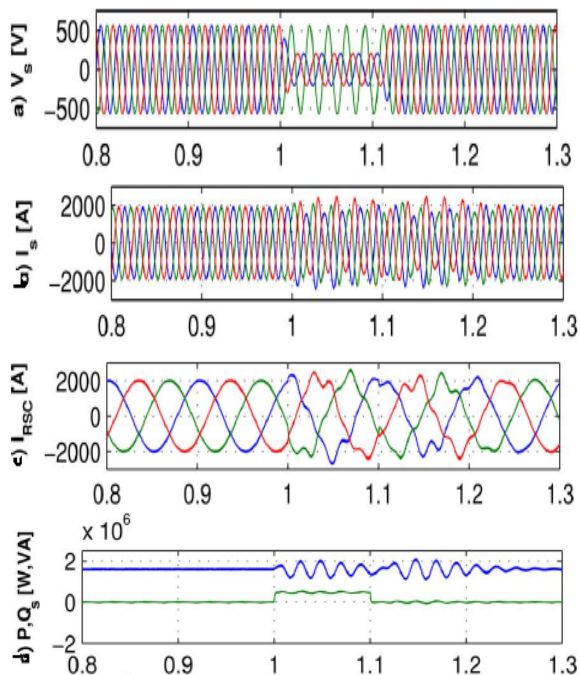


Fig. 12. Simulation results for the two-phase fault in the nominal value of 63%. a) grid voltage, b) stator current, c) rotor current and d) stator active and reactive powers [9].

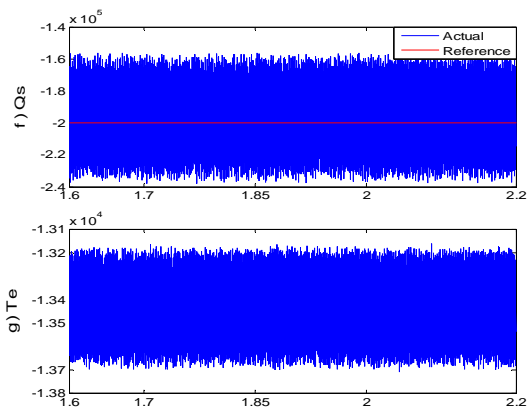
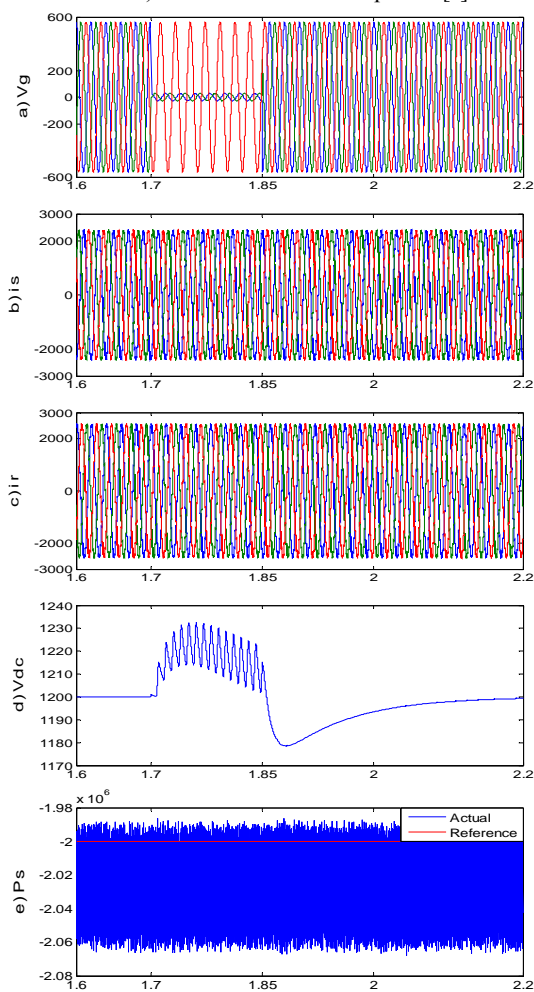
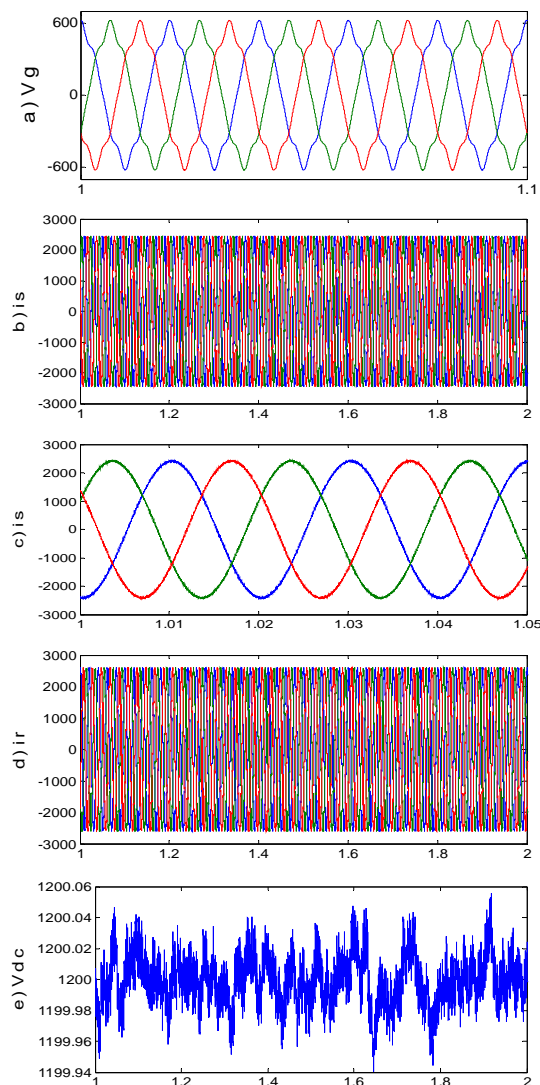


Fig. 13. Simulation results for the two-phase fault in the nominal value of 95%. a) grid voltage, b) stator current, c) rotor current, d) DC link voltage, e) stator's active power, f) stator's reactive power and g) is the electromagnetic torque.



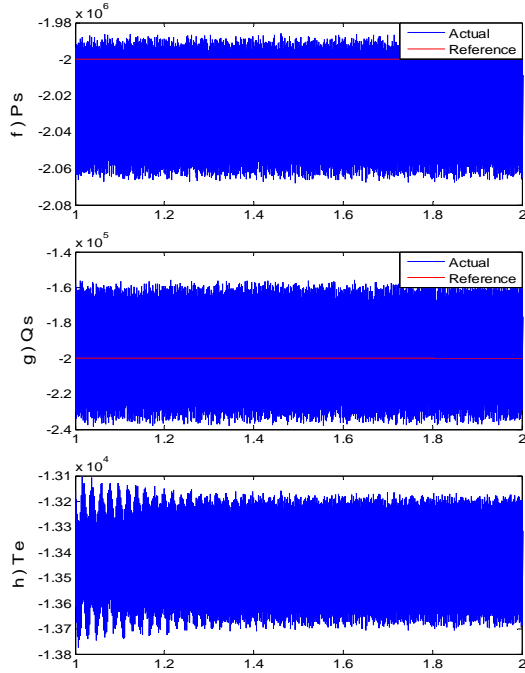


Fig. 14. Simulation results under harmonic distorted grid voltage. a) grid voltage, b) stator current, c) zooming stator current, d) rotor current, e) DC link voltage, f) stator's active power, g) stator's reactive power and h) electromagnetic torque.

Figure 14. c and h show that the problem of breaking torque and torque ripple are resolved by removing the fifth and seventh order harmonics. The stator and rotor currents in the three-phase windings are balanced while achieving the aforementioned object. (Fig. 14. b, d).

Test 5

In Fig. 15, the simulation results, similar to the two-phase are presented. The only difference is that the rotor and stator resistance is increased up to 40%. As the results show, except for the electromagnetic torque, the parameter's change does not affect the system performance.

In order to show the effectiveness of the proposed method, some control methods in different grid faults are compared and their results are reported in Appendix D. The amplitude of the stator and rotor over currents and the DC link voltage are calculated from their corresponding Refs. [9-13].

According to the results presented in Table. C, the voltage drop rate of the grid in the proposed method is considered higher than the other references, and has a better performance compared with the other published researches.

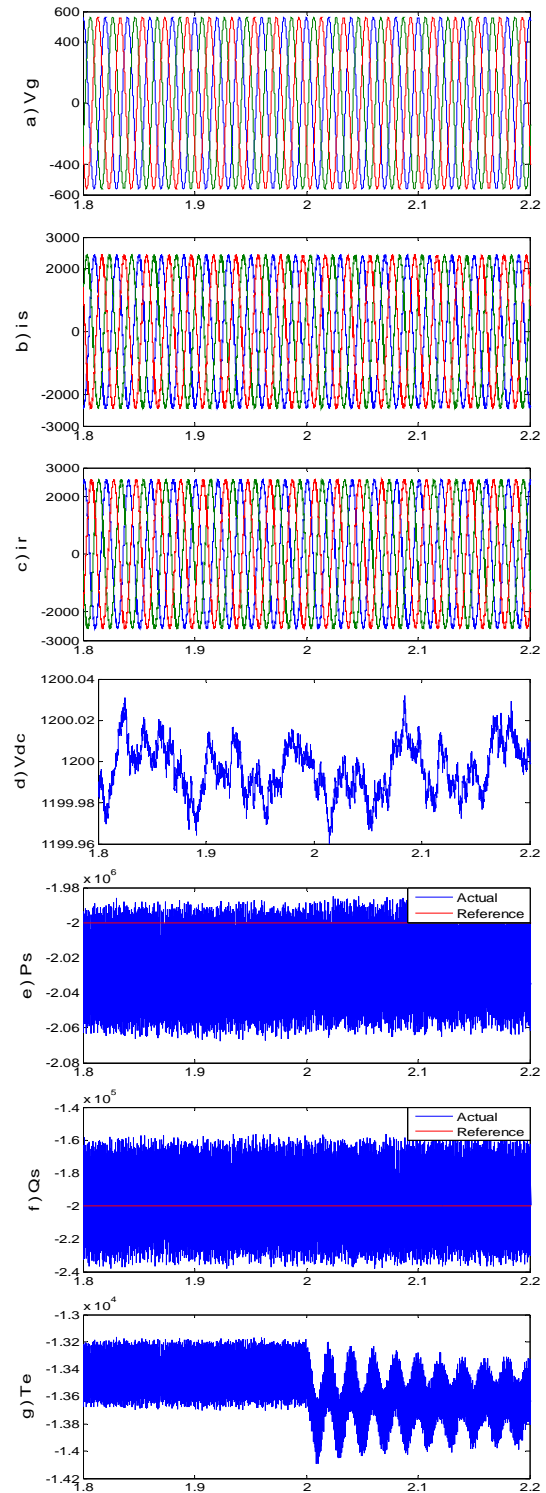


Fig. 15. Simulation results under parameter variations at $t=2s$. a) grid voltage, b) stator current, c) rotor current, d) DC link voltage, e) stator's active power, f) stator's reactive power and g) electromagnetic torque.

6. CONCLUSION

Since the grid regimes urge wind turbine generators to remain connected to the grid during the voltage drop conditions, a method to achieve the fault ride through condition is the application of series

compensators to stator voltage correction. In this paper, sliding mode control method has been proposed to control the back-to-back RSC and GSC and the series compensator converter. In addition, the DC link voltage and the active and reactive output powers of the generator are controlled and limits the rotor and stator over currents without using the crowbar resistors at the time of fault. Furthermore, this control method has an acceptable performance in all fault conditions without any change in controller's coefficients.

AS well as, the sliding mode method is robust to generator parameter variations due to its variable structure nature. Finally an effective comparison between the proposed method and some conventional techniques is presented. Simulation results show the effectiveness of the proposed technique.

APPENDIX

Table A.1. DFIG Parameters

Parameter	Value
R_s	10 m Ω
R_r	2.9 m Ω
L_{ls}	77.306 μH
L_{lr}	83.369 μH
L_m	3.7 mH

Vdc*	1200 V
R_g	0 Ω
C	7.5 mF
L_g	0.25 mH
Stator voltage (rms)	690 V
Rated Power	2 MW
P (pole pairs)	3

Table A.2. Controller coefficients

Parameter	Value
$k_{P_{s1}}$	10
$k_{Q_{s1}}$	10
k_{P_s}	20000
k_{Q_s}	20000
λ_1	1
λ_2	1
λ_{v_α}	1
λ_{v_β}	1
λ_{Qg}	1
$\lambda_{v_{\alpha 1}}$	100
λ_{v_β}	100

ACKNOWLEDGMENT

The authors would like to acknowledge the partial support of Esfahan Regional Electrical Company from this research work .

Table A.3. Comparing different structures for fault ride through control

FRT Scheme	Location series converter	Fault Type	The voltage drop	Over current rotor	Over current stator	DC- Link Over voltage
vector control and adaptive fuzzy for series converter [11]	grid	Tree phase	10%	60%	85%	4%
vector control and SCESS[12]	Stator terminal	Single phase	93%	100%	100%	Not checked
		Three phase	93%	105%	105%	Not checked
Vector control and Nine switch converter [13]	Stator terminal	Single phase	33%	5%	Not checked	10%
		Two phase	33%	5%	Not checked	10%
		Three phase	80%	10%	5%	10%
vector control and resonance for DVR[9]	grid	Two phase	63%	30%	20%	Not checked
vector control for all converter[10]	grid	Three phase	90%	18%	Not checked	4%
Proposed method With sliding mode control	Stator terminal	Two phase	95%	0%	0%	11.1%
		Three phase	95%	0%	0%	48%
		Grid voltage harmonic	V5=6% and V7=5%	0%	0%	0%

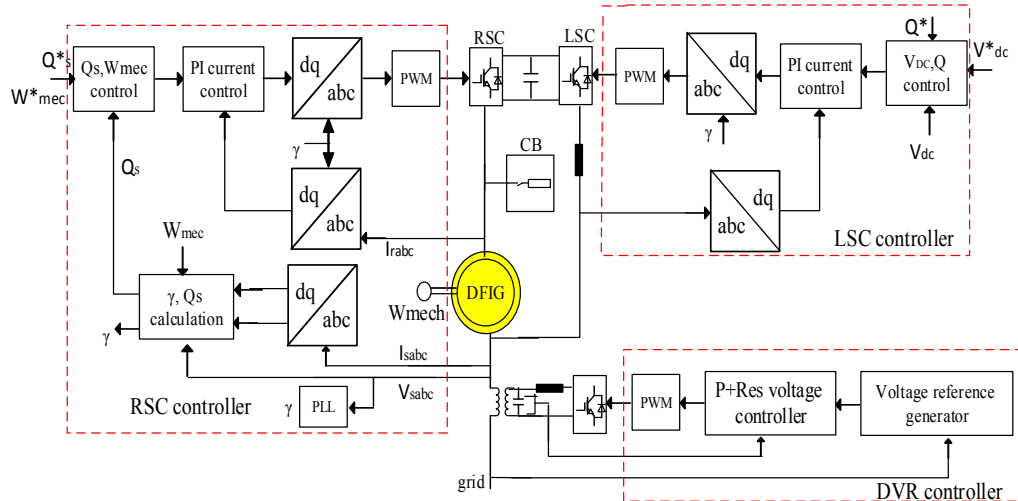


Fig. A. Fault ride through control based on vector control and dynamic voltage restore [9]

REFERENCES

- [1] H.T. Jadhav and R. Roy, "A comprehensive review on the grid integration of doubly fed induction generator," *International Journal of Electrical Power and Energy Systems*, vol. 49, pp. 8-18, 2013.
- [2] M. Tsili and S. Papathanassiou, "A review of grid code technical requirements for wind farms," *IET Proceedings on Renewable Power Generation*, vol. 3, no. 3, pp. 308-332, 2009.
- [3] A. Geniusz, S. Engelhardt and J. Kretschmann, "Optimised fault ride through performance for wind energy systems with doubly fed induction generator," in *Proceedings of the European Wind Energy Conference & Exhibition, Brussels*, pp. 1-9, 2008.
- [4] M. Rahimi and M. Parniani, "Grid-fault ride-through analysis and control of wind turbines with doubly fed induction generators," *Electric Power Systems Research*, vol. 80, no. 2, pp. 184-195, 2010.
- [5] A. H. Kasem, E. F. El-Saadany, H. H. El-Tamaly and M. A. A. Wahab, "An improved fault ride-through strategy for doubly fed induction generator-based wind turbines," *IET Proceedings on Renewable Power Generation*, vol. 2, no. 4, pp. 201-214, 2008.
- [6] J. Vidal, G. Abad, J. Arza and S. Aurtenechea, "Single-phase DC crowbar topologies for low voltage ride through fulfillment of high-power doubly fed induction generator-based wind turbines," *IEEE Transactions on Energy Conversion*, vol. 28, no. 3, pp. 768-781, 2013.
- [7] L. Peng and Y. Li, "Improved crowbar control strategy of DFIG based wind turbines for grid fault ride-through," *IEEE Transactions on Industrial Electronics*, vol. 40, no. 1, pp. 1932-1938, 2009.
- [8] M. Rahimi and M. Parniani, "Efficient control scheme of wind turbines with doubly fed induction generators for low voltage ride-through capability enhancement," *IET Proceedings on Renewable Power Generation*, vol. 4, no. 3, pp. 242-252, 2010.
- [9] C. Wessels, F. Gebhardt and F. Wilhelm Fuchs, "Fault ride-through of a DFIG wind turbine using a dynamic voltage restorer during symmetrical and asymmetrical grid faults," *IEEE Transactions on Power Electronics*, vol. 26, no. 3, pp. 807-815, 2011.
- [10] O. Abdel, B. Nasiri and A. Nasiri, "Series voltage compensation for DFIG wind turbine low-voltage ride-through solution," *IEEE Transactions on Energy Conversion*, vol. 26, no. 1, pp. 272-281, 2011.
- [11] E. El-Hawatt, M.S. Hamad, K.H. Ahmed and I.F. El Arabawy, "Low voltage ride-through capability enhancement of a DFIG wind turbine using a dynamic voltage restorer with adaptive fuzzy PI controller," in *Proceedings of the International Conference on Renewable Energy Research and Applications*, Spain, pp. 1234-1239, 2013.
- [12] I. Spyros, G. Kavanoudis and C. S. Demoulias, "FRT capability of a DFIG in isolated grids with dynamic voltage restorer and energy storage," in *proceedings of the IEEE 5th International Symposium on Power Electronics for Distributed Generation Systems (PEDGS)*, pp. 1-8, 2014.
- [13] B. B. Ambati, P. Kanjiya and V. Khadkikar, "A low component count series voltage compensation scheme for DFIG WTs to enhance fault ride-through capability," *IEEE Transactions on Energy Conversion*, vol. 30, no. 1, pp. 1-10, 2015.
- [14] L. Yang, Z. Xu, J. Østergaard, Z.Y. Dong and K. P. Wong, "Advanced control strategy of DFIG wind turbines for power system fault ride through," *IEEE Transactions on Power Systems*, vol. 27, no. 2, pp. 713-722, 2012.
- [15] M. Darabian, A. Jalilvand and R. Noroozian, "Combined use of sensitivity analysis and hybrid wavelet-psoanfis to improve dynamic performance of DFIG-based wind generation," *Journal of Operation and Automation in Power Engineering*,

- vol. 2, no. 1, pp. 49-59, 2014.
- [16] H. Khorramdel, B. Khorramdel, M. Tayebi Khorrami and H. Rastegar, "A multi-objective economic load dispatch considering accessibility of wind power with here-and-now approach," *Journal of Operation and Automation in Power Engineering*, vol. 2, no. 1, pp. 60-73, 2014.
- [17] M.I. Martinez, G. Tapia, A. Susperregui and H. Camblong, "Sliding-mode control for DFIG rotor and grid-side converters under unbalanced and harmonically distorted grid voltage," *IEEE Transactions on Energy Conversion*, vol. 27, no. 2, pp. 328-339, 2012.
- [18] L. Changjin, X. Dehong, Z. Nan, F. Blaabjerg and Ch. Min, "DC-voltage fluctuation elimination through a DC-capacitor current control for DFIG converters under unbalanced grid voltage conditions," *IEEE Transactions on Power Electronics*, vol. 28, no.7, pp. 3206-3218, 2013.
- [19] J. Vidal, G. Abad, J. Arza and S. Aurtenechea, "Single-phase DC crowbar topologies for low voltage ride through fulfillment of high-power doubly fed induction generator-based wind turbines," *IEEE Transactions on Energy Conversion*, vol. 28, no. 3, pp. 768-781, 2013.
- [20] G. Pannell, B. Zahawi, D.J. Atkinson and P. Missailidis, "Evaluation of the performance of a DC-link brake chopper as a DFIG low-voltage fault-ride-through device," *IEEE Transactions on Energy Conversion*, vol. 28, no. 3, pp. 535-542, 2013.
- [21] M. Wang, W. Xu, H. Jia and X. Yu, "A new method for DFIG fault ride through using resistance and capacity crowbar circuit," in *Proceedings of the 2013 IEEE International Conference on Industrial Technology*, pp. 2004-2009, 2013.
- [22] P. Cheng and H. Nian, "An improved control strategy for DFIG system and dynamic voltage restorer under grid voltage dip," in *Proceedings of the 2012 IEEE International Symposium on Industrial Electronics*, pp.1868 - 1873, 2012.
- [23] S. Zhang, K.J. Tseng, S.S. Choi, T.D. Nguyen and D. L. Yao, "Advanced control of series voltage compensation to enhance wind turbine ride through," *IEEE Transactions on Power Electronics*, vol. 27, no. 2, pp. 763-772, 2012.
- [24] P.S. Flannery and G. Venkataramanan, "Evaluation of voltage sag ride-through of a doubly fed induction generator wind turbine with series grid side converter," in *Proceedings of the IEEE Power Electronics Specialists Conference*, pp. 1839-1845, 2007.
- [25] V. Utkin, J. Guldner and J. Shi, "Sliding mode control in electromechanical systems," *London, U.K., Taylor and Francis*, 1999.
- [26] V. Utkin, "Sliding mode control design principles and applications to electric drives," *IEEE Transaction on Industrial Electronics*, vol. 40, no. 1, pp. 23-36, 1993.